THE JOURNAL OF PHYSICAL CHEMISTRY C

Article

Cite This: J. Phys. Chem. C 2019, 123, 26932−26938

pubs.acs.org/JPCC

Chain-Length-Dependent Reactivity of Alkanethiolate Self-Assembled Monolayers with Atomic Hydrogen

Jeffrey D. Sayler,[†] Sarah Brown,[†] and S. J. Sibener*

The James Franck Institute and Department of Chemistry, The University of Chicago, 929 E 57th Street, Chicago, Illinois 60637, United States

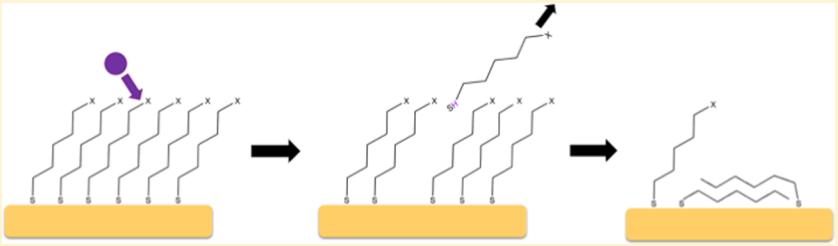

ABSTRACT: Gas−surface interactions are some of the most important yet complex chemical processes to occur, as they intrinsically involve many-body phenomena across a wide spectrum of energies and length scales. To understand these complicated interfacial interactions, we often use model systems such as thiolate self-assembled monolayers (SAMs) to study phenomena like reactivity and passivation, as these systems afford fine control over the surface parameters governing the events in question. In this study, we examine the effect of chain length on the reactivity of alkanethiolate SAMs with atomic hydrogen by monitoring morphological surface evolution throughout the reaction. These spatiotemporal data were obtained using ultrahigh vacuum scanning tunneling microscopy (UHV-STM) with directed in situ atomic hydrogen dosing. For a series of alkanethiolate SAMs 8- to 11-carbons long, we find that small increases in chain length cause disproportionately large decreases in reactivity. These reaction trends led us to develop a kinetic model characterized by two rate constants: a slow rate for hydrogen reactivity with close-packed domains, which is chain-length dependent, and a fast rate for reactivity with low-density regions, which is the same for all samples examined. In addition to reaction rates, we also tracked chain-length-dependent changes in surface morphology, notably how the size and shape of the SAMs' etch pits evolved following hydrogen exposure. Few differences were observed in the 10C and 11C samples, while there was a significant increase in the mean etch pit area of the 8C and 9C SAMs. Overall, this study provides important quantitative insights into how surface packing and dynamic disorder of organic thin films can influence their passivation capabilities.

INTRODUCTION

Thiolate self-assembled monolayer (SAMs) on Au(111) are some of the most well-studied systems in the surface science community.[1−4] These materials consist of densely packed organic molecules that are chemisorbed onto a metal substrate and arranged in a highly ordered two-dimensional (2D) polycrystalline structure. The tunability of the molecules' chemical functionality allows for the control of surface properties such as wetting,[5−8] adhesion,[7,9] photoactivity,[10] and chemical reactivity.[3] This versatility has enabled SAMs to be used in a variety of applications ranging from biomimetics[5,9,11,12] to corrosion inhibition.[13,14]

The versatility of SAMs has also popularized their use as model systems for studying gas−surface interactions. These are some of the most important yet complex chemical processes, as they intrinsically involve many-body phenomena across a wide spectrum of energies and length scales. However, this also means that they often require simplified model systems to facilitate their study. An appropriately selected SAM can hence be used to probe reaction dynamics as a function of surface parameters such as the chain length, chain parity, or chemical functionality.[15] For example, alkanethiolate SAMs have been used to explore the reactivity of atomic gases with hydrocarbons, which has importance for applications such as the passivation of electronic surfaces with organic thin films.[16,17]

Several groups have studied thiolate SAM reactivity with energetic gas species such as H,[15,18−25] O,[26−30] and O_3,[31−33] as adsorption energetics and reaction dynamics are of great interest to the surface science community. For example, techniques such as X-ray photoelectron spectroscopy[15,28] and reflection absorption infrared spectroscopy[26] have been used to explore the effect of chain length on the reactivity of alkanethiolate SAMs with atomic gases. However, these spectroscopic methods are limited to providing spatially averaged information about the reactive surface as a whole; they cannot identify how individual surface features evolve over the course of the reaction.

To study the nanoscale kinetics of chain-length-dependent alkanethiolate SAM reactivity, we must therefore employ a more localized technique such as scanning tunneling

Received: July 17, 2019
Revised: October 7, 2019
Published: October 23, 2019

DOI: 10.1021/acs.jpcc.9b06809
J. Phys. Chem. C 2019, 123, 26932−26938

microscopy (STM). The direct-imaging and nondestructive nature of scanning probe microscopy typically allows better investigation of the mechanistic details of such reactions. Furthermore, results from previous STM studies of thiolate SAMs already provide us with important information on how variables such as temperature,[3,34−37] local surface environment,[24] and exposure to reactive gases[19−24,27,30] will influence a SAM's film structure. For example, earlier work by Kandel's group[22] shows how 1-octanethiolate SAMs react with atomic hydrogen and how the resultant monolayer damage is characterizable with STM. In particular, this work emphasizes the key role that domain boundaries play in SAM reactivity as well as how the adsorbate overlayer restructures throughout the reaction. As discussed below, our work builds upon these early findings, including the formulation of a comprehensive kinetic model that quantifies the overall chain-length-dependent reactivity for the various SAM phases. Subsequent studies[20,21] also reveal some molecular-scale mechanistic details of this reaction, with a focus on how gold adatoms are incorporated into alkanethiolate SAMs during monolayer formation, findings with which we agree. Finally, STM studies of hydrogen's reaction with bulkier, substituted thiolates such as 1-adamantanethiolate[19] show that the incorporation of gold adatoms into SAMs is not unique to *n*-alkanethiolates; however, the reduced packing density of these substituted monolayers does impact how the thiol molecules bind to and organize on the surface.

Here, we present a comprehensive ultrahigh vacuum scanning tunneling microscopy (UHV-STM) study on how chain length impacts the microscopic surface reconstruction of alkanethiolate SAMs during their reaction with atomic hydrogen. We track the reaction progression of four alkanethiolate SAMs (8- to 11-carbons long) by monitoring the surface fraction of close-packed thiols remaining after each hydrogen exposure. This progression is then correlated with the time-evolving local structure of high- and low-density molecular domains. These data have allowed us to develop a model that quantitatively describes the observed kinetics for short-chain alkanethiolate SAMs. Furthermore, we address spatiotemporal correlations in these reactions by characterizing the surface rearrangements that occur in both the monolayer and underlying substrate, with emphasis on how these changes depend on alkanethiolate chain length. This study demonstrates the variances in the passivation efficacy of these organic thin films with respect to attack by atomic hydrogen.

EXPERIMENTAL SECTION

Experiments were performed at 295 K in a UHV chamber (base pressure $\leq 1 \times 10^{-10}$ Torr) that houses both an RHK 350 Beetle UHV-STM/AFM and a Mantis MGC-75 thermal gas cracker. The in situ gas cracker is located 80 mm from the sample and oriented 50° from the imaging stage's surface normal, which corresponds to a solid angle of 0.004 sr. All atomic hydrogen therefore arrive at the surface from the same direction and is controlled by a manual shutter.

The beam source produces atomic hydrogen by passing molecular hydrogen (backing pressure of 1×10^{-7} Torr) through a heated iridium capillary and subsequently collimating it. Under these conditions, we expect a cracking efficiency of approximately 90%[38] and a hydrogen flux on the order of 10^{12} H-atoms cm^{-2} s^{-1}. To prevent the STM tip from shadowing the surface, the microscope head was fully retracted from the sample during exposures.

We prepared our reactive thiolate SAMs using solution deposition on flame-annealed Au(111)-on-mica substrates from Keysight Technologies. The substrates were immersed in 1.0 mM solutions of 1-octanethiol (8C), 1-nonanethiol (9C), 1-decanethiol (10C), 1-undecanethiol (11C), and 1*H*,1*H*,2*H*,2*H*-perfluorodecanethiol in ethanol for 2.5 h at 60 °C. Samples were then rinsed with ethanol and dried in air prior to placement in the UHV chamber.

STM images were taken with a +0.70 V bias on the sample and a tunneling current set point of 10 pA. To obtain precise data on relative reaction rates between SAMs of different chain lengths, two 2.5 mm × 5 mm samples were adjacently mounted and dosed simultaneously for each reaction: a 1-decanethiol sample, to be used as a control between the different experiments, and a second SAM sample of the desired length (8-, 9- or 11-carbons long). We also mounted two 10C samples together in a control experiment and observed identical reaction profiles, thus confirming that both samples received the same exposure to hydrogen. This control also confirmed that there are no noticeable differences in reactivity due to variations in the Au(111) surface structure or SAM domain orientation relative to the gas flux. Finally, we performed all of our STM image processing using Gwyddion, an open-source software for SPM data analysis.[39]

RESULTS AND DISCUSSION

Figure 1 presents STM images of the reaction progressions of a 1-decanethiolate SAM during its reaction with atomic hydrogen. These images are representative of the data taken during each experiment, for all chain lengths. The zero-minute panel of Figure 1 shows the SAM prior to any atomic hydrogen exposure. Here, we see the typical features of a saturated alkanethiolate SAM on Au(111): The thiol molecules have self-organized into a standing-up hexagonal close-packed structure (Figure 2A) with a lattice constant of 0.50 nm and a c(4 × 2)R30° superlattice. The alkane tails of the thiol molecules are in trans configuration, tilted 32° from the surface normal, and the symmetry of the underlying gold lattice produces three degenerate molecular orientations.[3,40,41] From

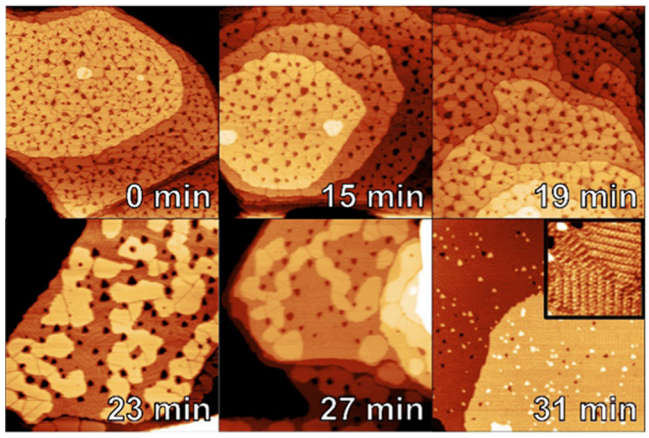

Figure 1. STM image progression (300 nm × 300 nm) of 1-decanethiolate SAM during its reaction with atomic hydrogen. At the end of the reaction, bright gold islands and low-density lying-down phase are visible on the gold substrate (see the inset 50 nm × 50 nm). The other three alkanethiolate SAMs (1-octanethiolate, 1-nonanethiolate, and 1-undecanethiolate) followed similar reaction pathways.

DOI: 10.1021/acs.jpcc.9b06809
J. Phys. Chem. C 2019, 123, 26932−26938

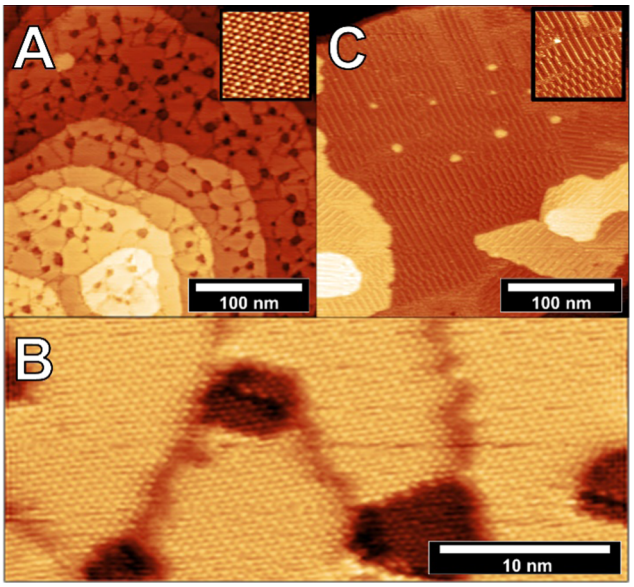

Figure 2. (A) STM image of an unreacted 1-decanethiolate SAM, with hexagonally close-packed domains separated by grain boundaries and etch pits. The inset (7 nm × 7 nm) shows molecular resolution of the thiolate lattice and the c(4 × 2)R30° superlattice. (B) Image of etch pits on a 1-decanethiolate SAM, where the close-packed hexagonal lattice is visible both inside and outside the pits. (C) Ordered low-density lying-down phase of 1-decanethiol. The inset (50 nm × 50 nm) shows bright and dark stripes corresponding to the aligned sulfur heads and the alkane tails, respectively.

this rotational degeneracy, the SAM acquires a polycrystalline structure in which single-crystal domains, 20−30 nm in diameter, are separated by grain boundaries. In these grain boundaries, we also find circular defects known as etch pits, which are gold vacancies created during the SAM's formation. It has been previously shown[20,21] that as the SAM forms, thiol molecules remove gold atoms from the substrate and incorporate them into the monolayer at a 2:1 thiol-to-gold ratio. This process leaves behind the etch pits with an average diameter of 5 nm, evenly scattered across the surface and filled with additional standing-up molecules (Figure 2B).

The later time points of Figure 1 show the morphological changes of the SAMs upon exposure to hydrogen. According to previous studies,[15] H-atoms will react with alkanethiolate SAMs in one of two ways: complete removal of whole thiols through the cleavage of the sulfur−gold bond or removal of hydrocarbon fragments via piecewise erosion. For longer alkanethiolates (C ≥ 12), reactivity is dominated by the latter mechanism. Hydrogen atoms react along the length of the hydrocarbon chains, which creates radical species and results in cross-linking between neighboring chains. This cross-linking slows the desorption of thiol molecules from the surface and causes hydrocarbon species to leave the surface in fragments. For shorter alkanethiolates (C ≤ 12), however, it is easier for atomic hydrogen to penetrate the thiolate film and directly attack the sulfur−gold bond.[15] We therefore expect to exclusively observe the sulfur−gold bond cleavage mechanism in our experiments. Moreover, our results suggest that when longer-chain thiols diminish in length due to repeated reaction with hydrogen, thiol removal via subsequent sulfur−gold bond cleavage may also become a significant reaction channel.

This reactivity initially presents itself as the thickening of grain boundaries, in agreement with the observations of previous studies;[20−22,24] as molecules leave the surface, lower-

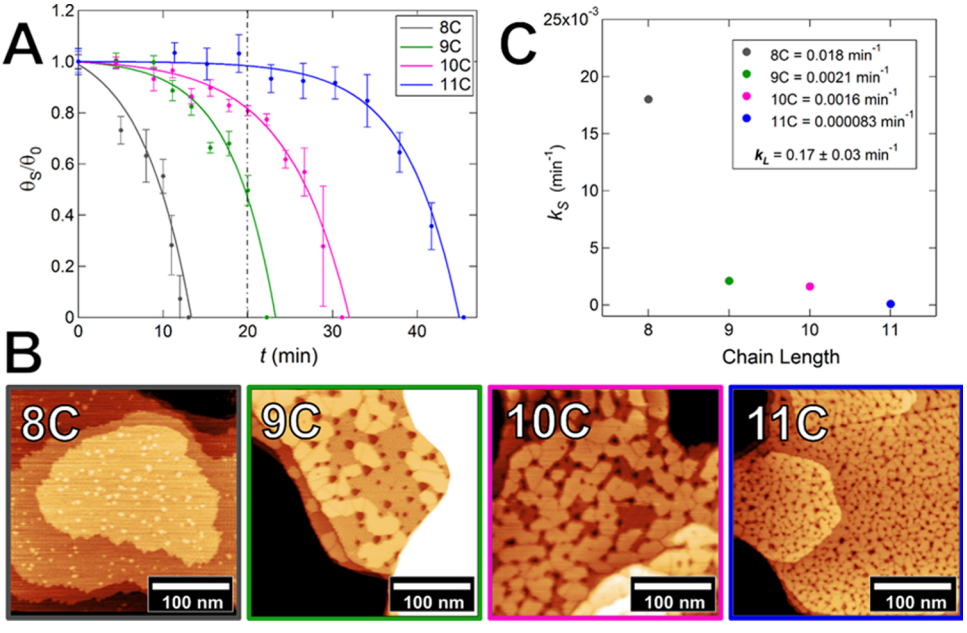

Figure 3. (A) Plot showing the fraction of standing-up phase coverage as a function of hydrogen exposure time. Each point is a weighted average of each sample's data collected at that time. Solid curves are fits produced using eq 4, and all experimental exposure times have been normalized to the common control sample (10C) to obtain relative reaction rates. The vertical dashed line marks the time at which we obtained the images shown in (C). (B) Representative images (300 nm × 300 nm) of the 8C, 9C, 10C, and 11C SAMs after 20 min of hydrogen exposure. At this time, there is a wide range of standing-up coverage between the different SAMs: The 8C sample has no standing-up phase left, which is evidenced by the bright gold islands covering the surface, whereas the 11C sample shows little evidence of reactivity, given its thin grain boundaries and numerous, evenly spaced etch pits. (C) Plot of rate constants for all four alkanethiolates, illustrating the nonlinear decrease in k_S associated with small increases in the chain length.

DOI: 10.1021/acs.jpcc.9b06809
J. Phys. Chem. C 2019, 123, 26932−26938

density thiolate phases begin to form and are observed in the STM images as darker regions. These low-density SAM phases include various disordered 2D fluid phases as well as ordered lying-down phases, which present as bright and dark stripes on the surface (Figure 2C).[2,34,36,42] Upon further exposure to hydrogen, the lower-density areas expand and interconnect, creating isolated puddles of standing-up phase. Eventually, no standing-up phase remains on the surface and small gold islands are formed from the Au atoms previously incorporated in the SAM.[20,21] We consider the reaction to be complete when no standing-up phase remains on the surface.

To quantify the reaction of alkanethiolate SAMs with atomic hydrogen, Figure 3A presents the area fraction of standing-up phase plotted as a function of hydrogen exposure time. We adjusted the exposure times for each reaction pair (10C and nC, where n = 8, 9, and 11) so that all decanethiolate times overlapped, enabling us to obtain relative reaction rates between all chain lengths. These data show that the rate of SAM reaction with atomic hydrogen decreases with increasing chain length, a fact that is also highlighted in Figure 3B where images of all four SAMs are compared at the same hydrogen exposure time. Remarkably, a chain length increase of a single carbon unit causes a disproportionately large decrease in the reaction rate; that is, a ∼10% increase in chain length corresponds to a 30% or greater decrease in reaction time (Figure 3C). It is also interesting to note that the reactivity does not depend noticeably on the parity of the carbon chains, despite even- and odd-numbered chains having terminal methyl groups with different orientations.[43,44]

According to the experimental data trends in Figure 3A, a SAM's reaction with atomic hydrogen accelerates as thiolates are removed from the surface. This implies that lower-density thiolate phases react more readily than close-packed molecules, in agreement with previous studies on octanethiolate SAMs which showed that reactivity is greater at defected sites such as grain boundaries and already-eroded regions.[22,24]

There are two different pathways through which the standing-up phase of a short-chain SAM can be consumed upon exposure to atomic hydrogen: the direct reaction of standing-up molecules (θ_S) with H-atoms, resulting in thiols leaving the surface (↑)

$$\theta_S \xrightarrow{k_S} \uparrow \tag{1}$$

and the conversion of the standing-up phase into lower-density phases (θ_L),[2,34,36,42] which then proceed to react with H-atoms

$$\theta_S \xrightarrow{k_{SL}} \theta_L \xrightarrow{k_L} \uparrow \tag{2}$$

Given that the conversion of standing-up molecules to low-density phase is much faster than the reaction of low-density phase SAM with H-atoms ($k_{SL} \gg k_L$), we can express the rate of standing-up phase erosion as

$$\frac{d\theta_S}{dt} = -k_S\theta_S - k_L\theta_L = -k_S\theta_S - k_L(\theta_0 - \theta_S) \tag{3}$$

where θ_S is the surface fraction of standing-up phase ($0 \le \theta_S \le 1$), t is the hydrogen exposure time, k_S is the rate constant for hydrogen's reaction with the standing-up phase, and k_L defines the rate of hydrogen's reaction with low-density phases. The final variable, θ_0, corresponds to the surface fraction of the standing-up phase at t = 0; note that this value is not equal to 1, as we exclude any area corresponding to initial defect sites such as etch pits and grain boundaries. Note that we also assume $\theta_0 = \theta_S + \theta_L$ for all t, as the thiolates' mobility on the surface at room temperature allows the approximation that non-standing-up phase regions will always be covered in some form of low-density SAM rather than bare Au(111).[34,36,42] Therefore, according to our model, we can express θ_S as a function of t as

$$\frac{\theta_S}{\theta_0} = A\, e^{-(k_S - k_L)t} + \frac{1}{1 - (k_S/k_L)} \tag{4}$$

where A is a constant dependent on k_S and k_L.

When reacting with the standing-up phase, atomic hydrogen must pass through the tightly packed alkane tails to reach the reactive sulfur at the surface. We have previously shown[26] that longer alkane chains produce a monolayer that is both taller and has fewer dynamic fluctuations, thereby hindering a gas molecule's progress to the surface. This implies that k_S should be strongly and inversely dependent on alkanethiolate chain length.

When reacting with the low-density SAM phases, atomic hydrogen has little-to-no steric barrier before reaching the sulfur head of the thiolates. In these regions, the monolayer thickness is independent of chain length. The reactivity of such areas should therefore be uniform across all four samples, and k_L should be the same for all chain lengths.

The solid curves in Figure 3A represent the fitting of the experimental data to eq 4, during which k_S and k_L remained free parameters. This process yielded k_S values ranging from 0.018 min^{-1} (8C) to 0.000083 min^{-1} (11C) and k_L values averaging at 0.17 ± 0.03 min^{-1}. Three major observations can be made based on these values. First, k_L varies minimally across chain lengths, a fact that agrees with our two-rate model and supports the proposal that k_L is independent of chain length. Second, $k_L \gg k_S$, which supports the expectation that regions covered with low-density phase are significantly more reactive than close-packed domains. Finally, as shown in Figure 3C, k_S decreases considerably with each additional carbon in the alkanethiol chain, which shows that hydrogen's ability to permeate standing-up phase decreases rapidly with increased chain length, more so than would be expected from a simple increase in monolayer thickness. This implies that greater rigidity and packing in the longer chains' crystal lattice plays an active role in the passivation of the gold substrate. This conclusion is further supported by observations in previous studies[15,19,26,45] as well as the results of analogous experiments where we reacted 1*H*,1*H*,2*H*,2*H*-perfluorodecanethiolate SAMs with atomic hydrogen. Although this SAM is of comparable thickness to the 1-decanethiolate monolayer, its chemical functionalization lends itself to a very different packing structure on the surface. Accordingly, the fluorinated SAM exhibited little-to-no reactivity after several hours of hydrogen exposure, unlike its hydrocarbon counterpart.

As previously mentioned, a major advantage of using STM for this study is that the reactions can be explored on a molecular level rather than being restricted to statistical averages. Figure 4 shows visual comparisons of all four SAM chain lengths, both before and after exposure to atomic hydrogen. Prior to reaction, the size and density of domains and etch pits are similar across the four samples. However, differences in etch pit size and distribution become evident in the 8C and 9C samples at θ_S = 0.5. For these shorter-chain monolayers, the etch pits grow larger, become more triangular, and decrease in density across the surface. Contrarily, the etch

DOI: 10.1021/acs.jpcc.9b06809
J. Phys. Chem. C 2019, 123, 26932−26938

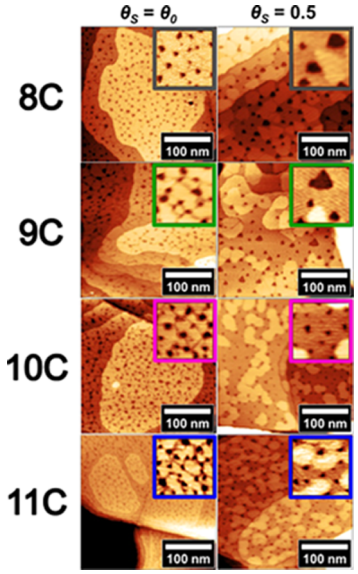

Figure 4. Representative 300 nm × 300 nm images of each alkanethiolate SAM (8C, 9C, 10C, and 11C) both prior to reaction and at $\theta_S = 0.5$. Square insets (50 nm × 50 nm) highlight the changes that we observe in etch pit morphology for each post-reaction sample. In the 8C and 9C samples, we find that the post-reaction etch pits are larger, fewer in number, and more triangular in their geometry compared to their initial counterparts. For the 10C and 11C samples, however, the etch pits are largely unchanged between the pre- and post-reaction samples; although their density across the surface decreases slightly, their small size and circular shape remain consistent.

pits of the 10C and 11C samples do not exhibit any major changes at $\theta_S = 0.5$. This result is quantified in Figure 5, where the distribution of etch pit sizes is presented for all chain lengths, both before and after hydrogen exposure. The 8C and 9C distributions shift noticeably at $\theta_S = 0.5$, indicating that there is an increase in the mean etch pit area for these SAMs post-reaction. The 10C and 11C distributions, however, remain largely unchanged after hydrogen exposure.

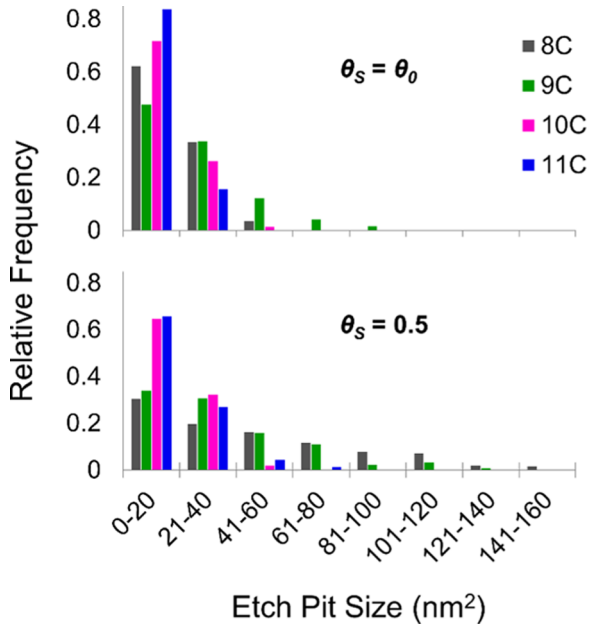

Figure 5. Histograms of etch pit areas for all four chain lengths prior to atomic hydrogen exposure (top) and at $\theta_S = 0.5$ (bottom). Shorter-chain SAMs show a larger growth in mean etch pit area, with increases of 33, 12, 2, and 5 nm^2 for 8C, 9C, 10C, and 11C, respectively.

Previous studies[30,45,46] attribute this etch pit restructuring to increased mobility of gold surface atoms upon the formation of low-density SAM phases. They propose that the formation of fewer, larger etch pits is the result of Ostwald ripening. However, our results in Figures 4 and 5 also suggest that the etch pits' degree of ripening depends strongly on thiolate chain length: 8C and 9C show the largest amount of gold substrate rearrangement, while 10C and 11C exhibit minimal restructuring. We can explain this trend by noting that the longer the alkanethiolate SAM, the stronger the van der Waals forces between neighboring chains.[15] Greater intermolecular forces reduce the likelihood of longer SAMs forming 2D fluid phases, thereby lowering both thiol molecule and gold adatom mobility across the surface.

CONCLUSIONS

We have successfully used the direct-imaging capabilities of STM to show that the carbon chain length of an alkanethiolate SAM greatly impacts its reactivity with atomic hydrogen. First, our experimental data shows that areas of low thiol density on the surface are more susceptible to hydrogen attack than standing-up domains. Based on this observation, we have successfully described the kinetics of the reaction using a two-rate model: one rate constant for hydrogen reacting with the standing-up phase (which is chain length dependent) and the other for hydrogen reacting with low-density regions (which is the same for all chain lengths). This model describes the behavior of all four chain lengths within statistical error and could be used to predict the behavior of other alkanethiolate SAMs in the short-chain regime. Second, we found that small decreases in the film thickness lead to disproportionately large increases in the reaction rate. This implies that the packing structure and chain-length-dependent fluctuations of thiolate SAMs play an active role in the passivation of the underlying gold substrate. Finally, we found that the size, shape, and density of the SAMs' etch pits changed noticeably over the course of the reaction with hydrogen and that these changes are dependent on thiol chain length. The 10C and 11C samples exhibited minimal etch pit rearrangement, while there was significant growth in the mean etch pit size for the 8C and 9C SAMs. These reconstructions are attributed to Ostwald ripening, and we conclude that the weaker intermolecular forces between shorter-chain molecules permit greater mobility and dynamic fluctuations of thiols and their corresponding gold adatoms. These fluctuations therefore allow for more surface rearrangement.

This STM study provides important insight into the passivation capabilities of organic thin films and how these abilities depend heavily on packing structure and dynamic disorder. Experiments designed to explore the complete dynamics of this reaction are ongoing, using cryogenic cooling and the kinetic isotope effect to perturb thiolate mobility and probe molecular fluctuations in alkanethiolate self-assembled monolayers.

AUTHOR INFORMATION

Corresponding Author

*E-mail: s-sibener@uchicago.edu. Tel.: 773-702-7193.

DOI: 10.1021/acs.jpcc.9b06809
J. Phys. Chem. C 2019, 123, 26932−26938

ORCID

S. J. Sibener: 0000-0002-5298-5484

Notes

The authors declare no competing financial interest.

†J.D.S. and S.B. contributed equally to this work and are co-first authors of this manuscript.

■ ACKNOWLEDGMENTS

This work was supported by the National Science Foundation, Grant Nos. CHE-1566364 and CHE-1900188. Support from the NSF-Materials Research Science and Engineering Center at the University of Chicago, Grant No. NSF-DMR-14-20709, is also gratefully acknowledged.

■ REFERENCES

(1) Ulman, A. Formation and Structure of Self-Assembled Monolayers. *Chem. Rev.* **1996**, *96*, 1533−1554.
(2) Poirier, G. E.; Pylant, E. D. The Self-Assembly Mechanism of Alkanethiols on Au(111). *Science* **1996**, *272*, 1145−1148.
(3) Poirier, G. E. Characterization of Organosulfur Molecular Monolayers on Au(111) Using Scanning Tunneling Microscopy. *Chem. Rev.* **1997**, *97*, 1117−1128.
(4) Häkkinen, H. The Gold−Sulfur Interface at the Nanoscale. *Nat. Chem.* **2012**, *4*, 443−455.
(5) DiMilla, P. A.; Folkers, J. P.; Biebuyck, H. A.; Haerter, R.; Lopez, G. P.; Whitesides, G. M. Wetting and Protein Adsorption on Self Assembled Monolayers of Alkanethiolates Supported on Transparent Films of Gold. *J. Am. Chem. Soc.* **1994**, *116*, 2225−2226.
(6) Meena Devi, J. A Simulation Study on the Thermal and Wetting Behavior of Alkane Thiol SAM on Gold (111) Surface. *Prog. Nat. Sci.: Mater. Int.* **2014**, *24*, 405−411.
(7) Gleiche, M.; Chi, L. F.; Fuchs, H. Nanoscopic Channel Lattices with Controlled Anisotropic Wetting. *Nature* **2000**, *403*, 173−175.
(8) Laibinis, P. E.; Whitesides, G. M.; Allara, D. L.; Tao, Y. T.; Parikh, A. N.; Nuzzo, R. G. Comparison of the Structures and Wetting Properties of Self-Assembled Monolayers of *n*-Alkanethiols on the Coinage Metal Surfaces, Copper, Silver, and Gold. *J. Am. Chem. Soc.* **1991**, *113*, 7152−7167.
(9) Raynor, J. E.; Capadona, J. R.; Collard, D. M.; Petrie, T. A.; García, A. J. Polymer Brushes and Self-Assembled Monolayers: Versatile Platforms to Control Cell Adhesion to Biomaterials (Review). *Biointerphases* **2009**, *4*, FA3−FA16.
(10) Kondo, T.; Uosaki, K. Self-Assembled Monolayers (SAMs) with Photo-Functionalities. *J. Photochem. Photobiol., C* **2007**, *8*, 1−17.
(11) Plant, A. L. Self-Assembled Phospholipid/Alkanethiol Biomimetic Bilayers on Gold. *Langmuir* **1993**, *9*, 2764−2767.
(12) Prime, K. L.; Whitesides, G. M. Adsorption of Proteins onto Surfaces Containing End-Attached Oligo(Ethylene Oxide): A Model System Using Self-Assembled Monolayers. *J. Am. Chem. Soc.* **1993**, *115*, 10714−10721.
(13) Zamborini, F. P.; Crooks, R. M. Corrosion Passivation of Gold by *n*-Alkanethiol Self-Assembled Monolayers: Effect of Chain Length and End Group. *Langmuir* **1998**, *14*, 3279−3286.
(14) Yourdshahyan, Y.; Zhang, H. K.; Rappe, A. M. N-Alkyl Thiol Head Group Interactions with the Au(111) Surface. *Phys. Rev. B: Condens. Matter Mater. Phys.* **2000**, No. 081405.
(15) Gorham, J.; Smith, B.; Fairbrother, D. H. Modification of Alkanethiolate Self-Assembled Monolayers by Atomic Hydrogen: Influence of Alkyl Chain Length. *J. Phys. Chem. C* **2007**, *111*, 374−382.
(16) Sieval, A. B.; Huisman, C. L.; Schönecker, A.; Schuurmans, F. M.; van der Heide, A. S. H.; Goossens, A.; Sinke, W. C.; Zuilhof, H.; Sudhölter, E. J. R. Silicon Surface Passivation by Organic Monolayers: Minority Charge Carrier Lifetime Measurements and Kelvin Probe Investigations. *J. Phys. Chem. B* **2003**, *107*, 6846−6852.
(17) Love, J. C.; Estroff, L. A.; Kriebel, J. K.; Nuzzo, R. G.; Whitesides, G. M. Self-Assembled Monolayers of Thiolates on Metals as a Form of Nanotechnology. *Chem. Rev.* **2005**, *105*, 1103−1170.
(18) Gorham, J. M.; Stover, A. K.; Fairbrother, D. H. Modification of 1H,1H,2H,2H-Perfluorooctyltrichlorosilane Self-Assembled Monolayers by Atomic Hydrogen. *J. Phys. Chem. C* **2007**, *111*, 18663−18671.
(19) Jobbins, M. M.; Raigoza, A. F.; Kandel, S. A. Adatoms at the Sulfur−Gold Interface in 1-Adamantanethiolate Monolayers, Studied Using Reaction with Hydrogen Atoms and Scanning Tunneling Microscopy. *J. Phys. Chem. C* **2011**, *115*, 25437−25441.
(20) Kautz, N. A.; Kandel, S. A. Alkanethiol Monolayers Contain Gold Adatoms, and Adatom Coverage Is Independent of Chain Length. *J. Phys. Chem. C* **2009**, *113*, 19286−19291.
(21) Kautz, N. A.; Kandel, S. A. Alkanethiol/Au(111) Self-Assembled Monolayers Contain Gold Adatoms: Scanning Tunneling Microscopy before and after Reaction with Atomic Hydrogen. *J. Am. Chem. Soc.* **2008**, *130*, 6908−6909.
(22) Kautz, N. A.; Fogarty, D. P.; Kandel, S. A. Degradation of Octanethiol Self-Assembled Monolayers from Hydrogen-Atom Exposure: A Molecular-Scale Study Using Scanning Tunneling Microscopy. *Surf. Sci.* **2007**, *601*, L86−L90.
(23) Lee, D. Y.; Kautz, N. A.; Kandel, S. A. Reactivity of Gas-Phase Radicals with Organic Surfaces. *J. Phys. Chem. Lett.* **2013**, *4*, 4103−4112.
(24) Kautz, N. A.; Kandel, S. A. Reactivity of Self-Assembled Monolayers: Local Surface Environment Determines Monolayer Erosion Rates. *J. Phys. Chem. C* **2012**, *116*, 4725−4731.
(25) Layfield, J. P.; Troya, D. Theoretical Study of the Dynamics of F + Alkanethiol Self-Assembled Monolayer Hydrogen-Abstraction Reactions. *J. Chem. Phys.* **2010**, *132*, No. 134307.
(26) Yuan, H.; Gibson, K. D.; Li, W.; Sibener, S. J. Modification of Alkanethiolate Monolayers by O(3P) Atomic Oxygen: Effect of Chain Length and Surface Temperature. *J. Phys. Chem. B* **2013**, *117*, 4381−4389.
(27) Waring, C.; Bagot, P. A. J.; Räisänen, M. T.; Costen, M. L.; McKendrick, K. G. Dynamics of the Reaction of O(3P) Atoms with Alkylthiol Self-Assembled Monolayers. *J. Phys. Chem. A* **2009**, *113*, 4320−4329.
(28) Wagner, A. J.; Wolfe, G. M.; Fairbrother, D. H. Atomic Oxygen Reactions with Semifluorinated and *n*-Alkanethiolate Self-Assembled Monolayers. *J. Chem. Phys.* **2004**, *120*, 3799−3810.
(29) Torres, J.; Perry, C. C.; Bransfield, S. J.; Fairbrother, D. H. Radical Reactions with Organic Thin Films: Chemical Interaction of Atomic Oxygen with an X-Ray Modified Self-Assembled Monolayer. *J. Phys. Chem. B* **2002**, *106*, 6265−6272.
(30) Waring, C.; Bagot, P. A. J.; Bebbington, M. W. P.; Räisänen, M. T.; Buck, M.; Costen, M. L.; McKendrick, K. G. How Penetrable Are Thioalkyl Self-Assembled Monolayers? *J. Phys. Chem. Lett.* **2010**, *1*, 1917−1921.
(31) Fiegland, L. R.; McCorn Saint Fleur, M.; Morris, J. R. Reactions of CC-Terminated Self-Assembled Monolayers with Gas-Phase Ozone. *Langmuir* **2005**, *21*, 2660−2661.
(32) Norrod, K. L.; Rowlen, K. L. Ozone-Induced Oxidation of Self-Assembled Decanethiol: Contributing Mechanism for "Photooxidation"? *J. Am. Chem. Soc.* **1998**, *120*, 2656−2657.
(33) Poirier, G. E.; Herne, T. M.; Miller, C. C.; Tarlov, M. J. Molecular-Scale Characterization of the Reaction of Ozone with Decanethiol Monolayers on Au(111). *J. Am. Chem. Soc.* **1999**, *121*, 9703−9711.
(34) Fitts, W. P.; White, J. M.; Poirier, G. E. Low-Coverage Decanethiolate Structure on Au(111): Substrate Effects. *Langmuir* **2002**, *18*, 1561−1566.
(35) Picraux, L. B.; Zangmeister, C. D.; Batteas, J. D. Preparation and Structure of a Low-Density, Flat-Lying Decanethiol Monolayer from the Densely Packed, Upright Monolayer on Gold. *Langmuir* **2006**, *22*, 174−180.

DOI: 10.1021/acs.jpcc.9b06809
J. Phys. Chem. C 2019, 123, 26932−26938

(36) Poirier, G. E.; Fitts, W. P.; White, J. M. Two-Dimensional Phase Diagram of Decanethiol on Au(111). *Langmuir* **2001**, *17*, 1176−1183.
(37) Camillone, N.; Eisenberger, P.; Leung, T. Y. B.; Schwartz, P.; Scoles, G.; Poirier, G. E.; Tarlov, M. J. New Monolayer Phases of *n*-alkane Thiols Self-Assembled on Au(111): Preparation, Surface Characterization, and Imaging. *J. Chem. Phys.* **1994**, *101*, 11031−11036.
(38) Mantis Deposition LTD. MCG75 Thermal Gas Cracker Operations Manual, 2017.
(39) Nečas, D.; Klapetek, P. Gwyddion: An Open-Source Software for SPM Data Analysis. *Cent. Eur. J. Phys.* **2012**, *10*, 181−188.
(40) Poirier, G. E.; Tarlov, M. J. The c(4 × 2) Superlattice of *n*-Alkanethiol Monolayers Self-Assembled on Au(111). *Langmuir* **1994**, *10*, 2853−2856.
(41) Widrig, C. A.; Alves, C. A.; Porter, M. D. Scanning Tunneling Microscopy of Ethanethiolate and *n*-Octadecanethiolate Monolayers Spontaneously Absorbed at Gold Surfaces. *J. Am. Chem. Soc.* **1991**, *113*, 2805−2810.
(42) Poirier, G. E. Coverage-Dependent Phases and Phase Stability of Decanethiol on Au(111). *Langmuir* **1999**, *15*, 1167−1175.
(43) Tao, F.; Bernasek, S. L. Understanding Odd−Even Effects in Organic Self-Assembled Monolayers. *Chem. Rev.* **2007**, *107*, 1408−1453.
(44) Wong, S.-S.; Takano, H.; Porter, M. D. Mapping Orientation Differences of Terminal Functional Groups by Friction Force Microscopy. *Anal. Chem.* **1998**, *70*, 5209−5212.
(45) Poirier, G. E.; Tarlov, M. J.; Rushmeier, H. E. Two-Dimensional Liquid Phase and the p × $\sqrt{3}$ Phase of Alkanethiol Self-Assembled Monolayers on Au(111). *Langmuir* **1994**, *10*, 3383−3386.
(46) Poirier, G. E.; Tarlov, M. J. Molecular Ordering and Gold Migration Observed in Butanethiol Self-Assembled Monolayers Using Scanning Tunneling Microscopy. *J. Phys. Chem. A* **1995**, *99*, 10966−10970.

DOI: 10.1021/acs.jpcc.9b06809
J. Phys. Chem. C 2019, 123, 26932−26938